Jurnal Teknologi

Full Paper

EXPERIMENTAL INVESTIGATION OF HEAT TRANSFER OF SUPERCRITICAL FLUID FLOWING IN A TUBE WITH TWISTED TAPE

Ameer Abed Jaddoa*

Electromechanical Engineering Department, University of Technology, Baghdad 00964, Iraq

Article history
Received
10 July 2022
Received in revised form
8 November 2022
Accepted
11 December 2022
Published Online
23 February 2023

*Corresponding author
Ameer.A.Jaddoa@uotechnology.edu.iq

Graphical abstract

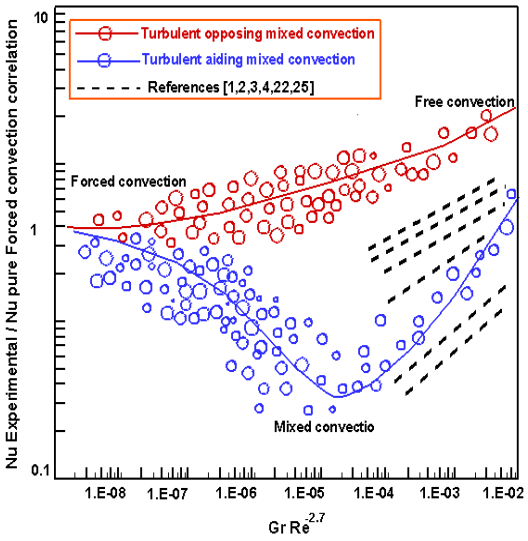

Abstract

An experimental study is introduced in this investigation to analyses the behavior of heat transfer in a cooled upstanding turbulent inflow environment of supercritical carbon dioxide. A combination of the method is utilized in dealing with empirical data obtained by a perpendicular tube with bending tape applied in the test model. In presenting the results, we adopted a common method 'the dimensionless constitution' throughout experimental procedures. Also, a development toward the correlation between the parameters is achieved for upward and downward inflows. The obtained outcomes could be supported and fill a gap presents in the previous studies on turbulent perpendicular composite heat load based on cooled circumstances. The empirical outcomes present the impact of buoyancy forces on the heat transfer operation. The recommendation of the present work is the develop a numerical model for supercritical CO_2 gas cooling in a tube with twisted tape.

Keywords: Composite heat load, Upward and downward flow, SC-CO_2, Pipe with twisted tape

1.0 INTRODUCTION

Over seventy years ago, numerous theoretical and empirical researches have been implemented utilizing supercritical fluids. Heat pumps, cryogenic engines, nuclear power plants or extraction processes are examples of such applications of industrial systems. In this vein, several works have been implemented based on horizontal tubes, vertically confined inflows, non-horizontal packed bed pipes, plumb annulus, plumb normal circular pipes, pipeline installations, and tiny-porous patterns [1-4].

To use supercritical fluid carbon dioxide (SC-CO_2) in a cooling system as well as in an energy circulation requires pre-defined procedures for the heat transfer operation. According to global agreements and European lawmaking, systems deemed harmful to the environment will be gradually eradicated. Consequently, alternative resources such as the use of natural substances to be used in refrigerants gained more concentration. One of the most candidate materials which characterize an environment friendly is carbon dioxide (CO_2). Owing to its characteristics represented by zero ozone depletion possibility and

mitigation of exacerbating the global warming, and its heat transfer capabilities features [5].

The absence of distinct fluid and vapour states and the significant fluctuations in the thermodynamic and material features at various heat degrees and pressures are the key features that are seen above the vital juncture. At a constant pressure of 80 bars for CO2, Figure 1 illustrates the impact of heat degree on a certain heat Cp, thermal conductivity k, dynamic density, and bulk density q. The Refprop 7.0 program was used to assess each thermophysical property [6]. Utilizing the formula created by [7], the density and specific heat are shown, while the density and thermal conductivity are calculated using [8].

These investigations can be regarded as important resources for analyzing the SC-CO_2 characteristics [9]. The spacer impact upon supercritical fluid of heat transfer SCHT was the subject of an existing work by the author introduced in [10]. They discovered that inflow obstacles often improve heat transfer (HT) and that the coolant heat degree was close to its pseudo-critical value upon the HT improvement was greatest (often surpassing 100%). Additionally, it was shown that considerable up-flow HT increase occurs downstream of panel separators. In a down-flow, meanwhile, the impact of grid separators on heat transmission was less noticeable and occasionally non-existent. Moreover, the research described in [11] used computational Fluid Dynamic (CFD) identifiers to anticipate spacer impacts on SC-HT. For normal HT conditions, these predictions were observed to be in reasonable agreement with empirical observations, but they were regarded to be of doubtful precision for HTD situations [11]. Considering the paper by [12] on CO2-cooled directly heated tubes, the current empirical inquiry is a continuation of the empirical program at the University of Ottawa. The main goal of that experiment, which was conducted concurrently, was to add more information to a trans-critical multi-fluid look-up table [13] for HT factors. Researchers looked at convective HT in SC-CO_2 inflows in tubes with and without inflow barriers [14]. Under specific circumstances, both the naked tube and the tube equipped with obstacles showed signs of HT deterioration (HTD).

The fluctuation of the SC HT factor with bulk enthalpy was found to be substantially influenced by changes in mass and HFs, but rather insensitive to changes in inlet heat degree and pressure, according to an analysis of the parametric trends. The fact that SCHT seems to be less dependent on MF under HTD circumstances is a significant discovery in the bare tube investigations. A significant tube with an inner diameter of 14.5 mm was explored for an empirical evaluation of HT in plumb upward SC-CO_2 inflow [15]. The intake specifications included an inlet pressure of 7.73 to 8.53 MPa, an HF of 20.66 to 125.14 kW/m^2, and an MF of 393.7 to 940 kg/s (m3s). Four relationships and the flotation variables Bo and Bo* were assessed using the empirical values. The Watts relationship was used to normalize the empirical Nu, and Bo was selected to represent the influence of flotation. We discovered that all investigated correlations demonstrated comparable forecast performance on the overall Nu. When Bo surpassed 105, which coincides with Jackson and Hall's threshold, a considerable reduction in the normalized Nu indicating HT deterioration (HT) was seen; the effect of flotation on HT began to lessen when Bo hit 10^4. To forecast the heat transport behaviours responsible for flotation, a segmented relationship was put out. By adding a dimensionless tube diameter component along with deteriorating standards from various diameters, a universal criterion was created, albeit the validity still requires additional empirical information from various diameters to confirm and improve. SC-CO_2 was uniformly heated in horizontal circular smooth tubes with inner diameters of 1.0 mm, 0.75 mm, and 0.5 mm to study the local heat transport properties of the gas [16].

The empirical outcomes showed that liquid heat degree rose prior to the pseudo-critical point and that heat transmission decreased immediately after the pseudo-critical point, illuminating the enhancement of HT. As a consequence of As a result of the augmentation of turbulence brought on by the drop in fluidity, the HT factor incremented once again when the liquid heat degree was adequately greater than the pseudo-critical value. Additionally, this work looked into how the parameters of outlet pressure, HF, MF, inlet heat degree, and tube diameter affected local HT. When the outlet liquid state was near the appropriate pseudo critical point, at which both the specific heat and Prandtl number hit peak values, the unit displayed the ideal heat fliuid (HF) with maximum thermal efficiency. The unit that had a larger mass flow rate (MF), a lower input temperature, or a smaller diameter demonstrated better (HT) performance when the other variables were held constant.

The local Nusselt number of $SCCO_2$- along the inflow channel in uniformly heated horizontal tubes can be accurately predicted by a novel experimental relationship constructed based on the empirical results. Predicting S-heat CO_2's transfer factor is still difficult owing to its complicated thermophysical features [17], particularly in heating settings with high HF to MF ratios (q/G). In this context, the HT of S-CO_2 is empirically examined in this mini pipe (d = 2 mm) on the scale of p = 7.6-8.4 MPa, q = 100-200 kW/m^2, and G = 400-700 kg/m^2 s, with the proportion of q/G being within 250-500 J/kg. Also, the variable effects on S-heat CO_2's transfer factor are examined. According to the results, it was discovered that pressure has little bearing on the HT factor, which declines with rising heat flow and falling MF. High q/G circumstances have an adverse impact on the heat transmission throughout the entire model and have a strong flotation impact. In this vein, the empirical data set for SC-CO_2 were compared with the existing HT relationships, however, these relationship prediction errors were generally quite significant, particularly in pseudo-critical locations.

As a consequence, a novel HT relationship for SC-CO_2 under high q/G situations is created, taking into consideration both the floatation impact and

changes in thermophysical characteristics. Additionally, SC-CO_2-induced convective HT and flow properties in a water-cooled empirical were explored [18] for good heat interchange modeling and evaluation. Additionally, utilizing the computational liquid dynamics approach in ANSYS CFX, counter-inflow tube-in-tube HX were computationally investigated utilizing three-dimensional Reynolds-averaged Navier-Stokes formulas and the shear stress transport (SST) turbulence prototype. Also, the impacts of SC-CO_2 inlet pressure, MF, tube diameter, and wall HF on SC-CO_2 mean HT factor were examined using a single tube prototype of the HX. Next, the wall temperature of conservative and hybrid values in CFX-Post on MHTC, the effects of turbulence prototypes and discretization methods on the advection terms in the SST prototype, and the flotation impact in the horizontal HX were all elucidated. In this vein, the empirical mean HT factor of SC-CO_2 can be more accurately predicted by the SST prototype than by the other approaches. By using the secondary flows in the tube, the flotation impact can enhance MHTC. In this vein, SC-CO_2 flowed in a vertically heated small pipe with an inner diameter of 2 mm and was tested empirically for its heat transport characteristics [19].

Wherein the empirical was run at 7.5–9 MPa pressure, low (G 200 kgm^2s1)/high (G > 200 kgm^2s^1) MF, and HF of 45–300 kWm^2. Also, convective HT was addressed concerning operational variables, flotation force, and inflow velocity. The findings demonstrated that even though the heat load (q/G) was substantial, there were no clear signs of HT deterioration at low MFs. The analysis process of HT features is needed to promote its application, wherein SC-CO_2 in different cross-section tubes requires analysis. In this context, three horizontal heat exchange tubes, including a straight tube, a converging tube, and a diverging tube, were presented in [20]. To study the HT in heat load performance of SC-CO_2 in the horizontal tube with different sizes under heating circumstances, we employed mathematical models. Upon comparison to a tube with a homogeneous size, the diverging tube efficiently improves overall HT outcomes.

Additionally, upon comparing to a straight tube, the rate of heat transmission is enhanced by 19.26%. On contrary, the converging tube reduces the efficiency of HT. Additionally, in order to highlight the fluid's HT deterioration process close to the top bus, we presented quasi-air film and eddy blockage concepts. Where SC-CO_2, which produces near top bus and has a low thermal conductivity similar to air at room temperature, is present in large quantities in the quasi-air film. Additionally, the Nu-based assessment reveals that the eddy blockage can worsen the HT performance at the top of the horizontal tube by 17%. This criterion variable, However, was suggested by double adjustments of density and temperature for determining the occurrence of eddy blockage. The dual impact of quasi-air film and eddy blockage on this account clarifies the physical process of HT degradation under the heating situation. This suggests that investigating the HT process in refrigeration plumb inflows while accounting for the impacts of flotation forces is a worthwhile area of research, not only for structures like heat pumps or air conditioners but also to fill in the gaps in knowledge regarding composite heat load under temperature condition. The goal of the current work is to carefully examine how inflow obstacles affect SC-HT. The findings of this study close the information gap that exists currently regarding SC-HT downstream of obstructions and could be applied to determining the thermal-hydraulic effect of fuel bundle spacers in SCWRS.

2.0 EXPERIMENTAL METHOD

The tests-work of flowing at SCF pressure for limited inflow integrated with measuring equipment is displayed in this section. In what follows, we present the investigation of HT through convection for the system shown in Figure 1 (a, b, c).

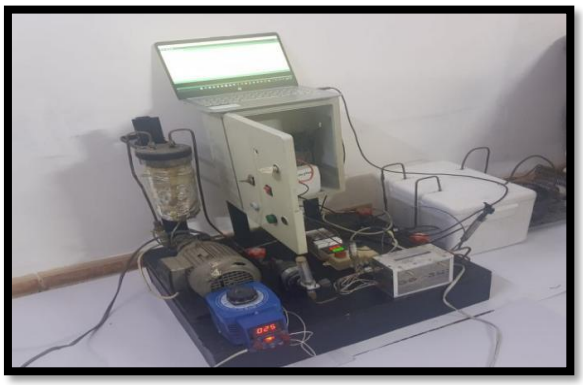

Figure 1a Experiential system of SC-CO_2 (Photo)

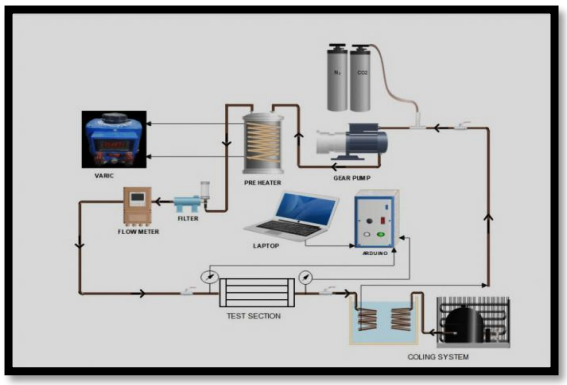

Figure 1b Experimental setup of SC-CO_2 (schematically)

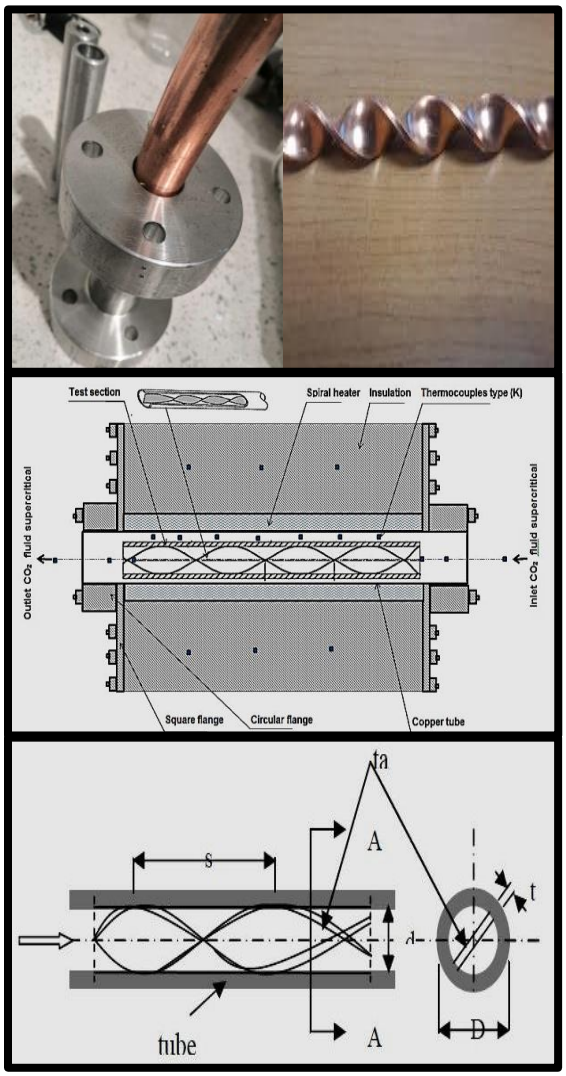

Figure 1c Experimental setup of SC-CO2 (test section))

The tube with twisted tape is depicted in Figure 1(c). The handbook stated that it was constructed from copper tube 360 alloys with dimensions of 50 mm in length and 8 mm in diameter. The bent tube is comprised of bent tubes with copper strips that are 2 mm thick, 45 mm long, and 2 mm wide (6 mm). The relationship between one length of twist and one length of the pitch (s) to the inner diameter of the tube is known as the twist ratio (TR) (d). The average between the bulk temperatures at the inlet and outlet was used to derive the liquid characteristics. With and without the insert, an empirical was run under continuous HF circumstances. CO_2 with a purity of 99.7% is kept in the CO_2 container. Ammonia gas is compressed by the device's compressor for use in the cooling regime. But when a compressor compresses a pressurised gas, it heats up (turns amber). It is worth indicating that ammonia gas was heated using the coils to dissipate heat. The gas will then be converted into an ammonia solvent under high pressure after condensing (becoming dark blue).

The high-pressure ammonia liquid then flows through a small hole that is sealed up in the expansion valve. The pressure on the exterior side of the hole is higher than on the inside side due to the compressor that extracts the gas from this place. As a consequence, the ammonia liquid reaches its heating degree and transforms into gas, becoming pale blue due to evaporation, with an ammonia vapour temperature of about 27 degrees Fahrenheit. The loop should be broken by heating the ammonia again when it starts to cool. One of the most crucial difficulties with the refrigeration unit is the choice of coolant components. The use of ethylene glycol gas as a refrigerant gas in this research is also justified by a number of factors, including heat degree control and decline, liquid properties at high-temperature levels in addition to its cost, and the capacity of gas toxicity with regard to environmental concerns, and flow ability. All of the work's elements, including the handle, springs, fixings, and screws, were made of stainless steel. The handle's function is more crucial since it stops the stem from losing and going out. Additionally, two powerful components were used to keep the stem sturdy and versatile. Additionally, the double-sided weep apertures are intended to easily find scheme leaking, while the packing gland/body thread was employed to withstand vibration. Additionally, the pressurize was recorded using a measuring device of the Bourdon tube pressure gauge PG23HP-P with a 1% precision (German manometers). High pressures up to 500 bar can be evaluated using this instrument. The actuator's front side is protected in the event of a device breakdown, and all other components—aside from the device's back—are in good working order. All of the equipment utilized in this study was reliable under static and dynamic pressure. Furthermore, a TSI of 5210-7 as an MF Multi-Meter was utilized to measure a wide scale of flow and record the flow average in bi-direction with a measurement accuracy of 2%. Integrating thermal and pressurized sensors was used to adjust for the intake irrespective of temperature degree or pressure in order to increase the precision of the observations. In addition to the capabilities of the sensor elements whether for absolute pressurize or temperature the apparatus might also capture the overall amount by utilizing integrated aggregates. In this vein, to detect the pressurize variation of flows at the flow recorder or anyplace along the channel, a differential pressurize detector, model 5210-7, was added to the bulk flow measurements equipment.

Additionally, the flow recorder can estimate from 0 to 30 L/min with a 2 per cent accuracy. The totalizer's ability to accurately record volume depends on the trigger pressurize and heat level. In this experiment, a data logger was used. A defined data processor called the data recorder stores data as it is captured and shows it right away on the flow meter. In this context, the measures that were used for exact measurement were conducted on metering the flow of Carbon dioxide, measuring the gas volume, pressurizing, as well as conserving and recording data,

making this work a prototype for assessing CO_2 models.

The digital screen, which stands out for having a color display and being touchable, can show four measurements of CO_2 flowing at once. With flow measurement, the device measures right away and is simple to set up and operate. For the purpose of managing the gas inflow meter, the FLO-Sight program was installed and connected to the computer. Thus, it indicates that the settings and methods for displaying the advanced data were chosen.

Furthermore, the Lm35 analogue linear sensor, which measures one degree Celsius every ten millivolts, is another sensor to detect utilized to measure heat levels. In addition, the heating operations were managed using the Arduino Uno micro-controller. It is important to note that the input voltage range of 0 to 5 volts and the 10-bit storage range of 0 to 1023 are proportional to changes in temperature. Wherein, every 2 degrees Celsius throughout this project, the heat will be proportionate to the voltage via Arduino, until it hits the highest quantity detected by the Lm35. Another temperature sensor, thermocouples type k, which was developed at a time when metallurgical research was more advanced, was used to analyze the behaviour of the prototype heat degree. Since the collection temperature is between -200 and 1350 °C or -330 and 2460 °F in this case, several sample attributes may vary. Thermocouples, also referred to as type k thermocouples are electrical apparatus connected by a cable that depends on variations in bi-semiconductors. Also, the thermoelectric impact, which is reliant on voltage and heat degree, has an impact on the heat point as a result.

One type of heat detector that is frequently used is the thermocouple. Other characteristics of thermocouples of kind K are their chrome-alum construction and linear sensitivity of 41 V/°C. The rationale for this is that the thermocouple detector is comprised of nickel, a magnetic material that deflects the output upon it hits the Curie point, which for thermocouple detector K occurs at a heat point of 185 per cent. It is worth mentioning that carbon steel was utilized to make the filter housing (FH), which is utilized to extract CO_2. The FH is capable of withstanding 100 bar of pressure. A Nichrome heating element, which is composed of 20% chromium and 80% nickel, can be used due to the model's high heat degree to protect the cables from damage and breaking. It also has oxidation resistance and the capacity to form a coating of chromium oxide once heated. The Nichrome heating element can also be utilized as a tape with a 10 m length, 6.8 A current, and 1500 W power output. This work used the AC converter 520T-10, also known as a Variac, which has a current and voltage of 10 A and 130 volts, respectively. The input voltage of 110 volts. This device has three output sockets and connection connections.

Since it is composed of recyclable material fibres in the range of 75 to 85%, cellulose was used as a thermal insulator and is one of the least harmful ones available. The remaining 15% is composed of fire retardants such as ammonium sulphate or boric acid. Cellulose is one of the most essential fire-fighting compounds and one of the most non-toxic insulators due to its compressed form, which prevents oxygen from entering and limiting the damage induced by fires. Due to its high thermal and electrical conductivity, ductility, and malleability, the experimental component was constructed from 99.5% pure copper, which has an atomic number of 29. Pure copper is pinkish-orange in colour on its exposed surface.

Copper is utilized in many different industries, including the manufacture of devices, tokens, marine hardware, and measurement equipment. This is because it is a cheap substance that is also added to various metal alloys to create jewellery like sterling silver, particularly because it has the ability to transfer heat and electricity.

3.0 DATA REDUCTION

The overall HT factor (H) for the whole length of each subsection that has been cooled down is frequently estimated utilising the LMTD approach (Log Mean Temperature Difference), as shown below[26]:

$$Q^{\rightarrow} = LMTD \times H \times A \tag{1}$$

The average temperature logarithm of different LMTD for opposite inflow take the expression as [26]:

$$\text{LMTD} = \left[\left(T_{out,CO2} - T_{in,water}\right) - \left(T_{in,CO2} - T_{out,water}\right)\right] \times lin\left(\frac{T_{out,CO2} - T_{in,water}}{T_{in,CO2} - T_{out,water}}\right)^{-1} \tag{2}$$

The temperature differential between the low temperature water and the Carbon dioxide fluctuates non-linearly with convection and distance from the model's input due to the strong temperature dependence of the thermo-physical feature of Carbon dioxide. The traditional logarithmic mean rate equation was thus preferred to an integral technique suggested by [21,22]. The heat inflow rate between cold water and CO2 DF can be expressed by using an infinitesimal portion $DQ^{\rightarrow}$ of the model's exchange surface:

$$DQ^{\rightarrow} = H \times (T_{water} - T_{CO2})\text{DF} \tag{3}$$

Where H represents the general HT factor between CO_2 and water. The following formulas are used to calculate the average total HT factor along each models under investigation whole length:

$$H = \frac{1}{F} \times \int_O^F \frac{\text{DQ}^{\rightarrow}}{T_{water}\text{DQ}^{\rightarrow} - T_{CO2}\text{DQ}^{\rightarrow}} = \frac{1}{F} \times \int_O^F H \,\text{DF} \tag{4}$$

An approximate constant water heat degree through the test length was achieved for all empirical settings

since heat degree differences on the water side were smaller than 3 °C:

$$T_{water}\mathrm{D}Q^{\rightarrow} = T_{water} \quad (5)$$

The changing temperature of infinitesimal zone dS gives the following expression

$$\mathrm{DF} = \varepsilon\,(\mathrm{dh})_{CO2} \quad (6)$$

Where (h) denotes the certain enthalpy of the SC-CO_2. By some simplifications steps eq.4 to eq.6 turn out to be the overall HT factor over the whole length of the model under investigation:

$$\mathrm{H} = \frac{\varepsilon}{F}\int_{h_{in}}^{h_{out}}(T_{water} - T_{CO2})^{-1}\,dh \quad (7)$$

The HT factor on the carbon dioxide side is computed from the overall HT factor as:

$$\frac{1}{H}\frac{1}{\alpha_{CO2}} + lin\frac{d_{ext.}}{d_{in.}} \times \frac{F_{exchange,internal}}{2\pi l\beta_x} + \frac{F_{exchange,internal}}{F_{exchange,external}\times\alpha_{water}} \quad (8)$$

As cited earlier, divergences of cooling water heat degrees were generally lower than 3 C for all models under investigation, permitting us to consider the water feature to be stable throughout the entire experimental procedure. In Figure 2, for upward inflows, the integral technique-based Carbon dioxide side HT factor was contrasted with the value determined using the widely used LMTD approach. While, in descending flows, the same behavior is seen. The principal variations between the integral and LMTD approaches are concentrated near the pseudo-critical temperature Tpc for all pressures, and these discrepancies become less significant as pressure rises. In this vein, these findings pertain to the relationship between the specific heat Cp of supercritical CO_2 and changes in heat degree and pressure. The quantity of C_p peaks at pseudo-critical temperature T_{pc}, and the size of this crest decreases with rising pressure. In Figure 3, the HT factors derived using the two approaches were directly compared at various pressures and a downward MF of G = 750 kg/m^2 s. Also, variations are noticed for pressures of 75 bars and 95 bars near Tpc, but no appreciable variation is seen in the fluid or gas-like areas. Moreover, the selection of the data deduction technique does not result in appreciable changes throughout the whole temperature range at the high pressure of 115 bar and 135 bar. Furthermore, the variances between the integral and LMTD methods typically do not surpass 3% outside of the pseudo-critical temperature Tpc and 7% inside the pseudo-critical area. Also, upon the mass heat degree was near Tpc, there were merely minor heat degree changes of the CO_2 along the test section (less than 3 °C), while, when the mass heat degree was distant from the pseudo-critical temperature, bigger variances were observed (greater than 6-7 °C).

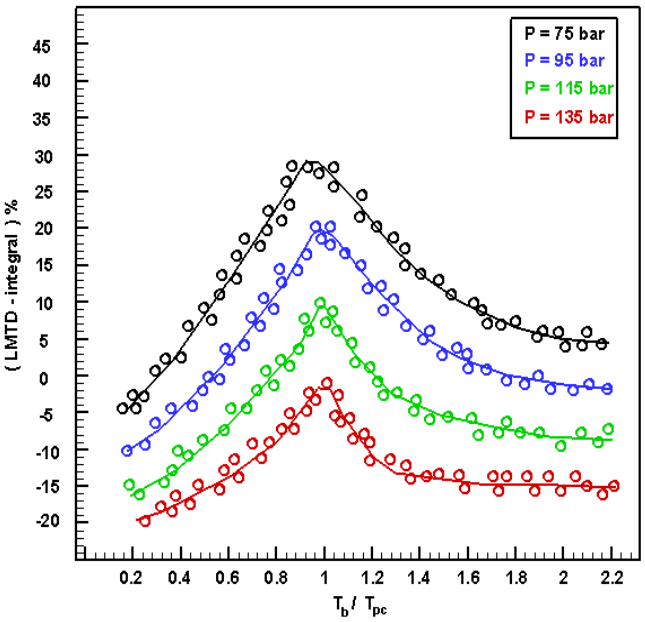

Figure 2 Difference between LMTD and integral method for different pressures, upward flows

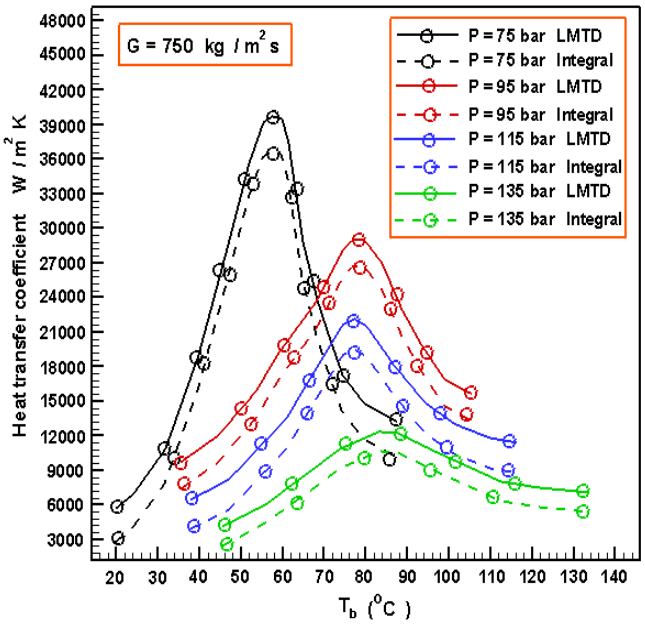

Figure 3 Comparison of heat transfer coefficient for integral and LMTD methods, downward flows

The precision of the HT factor was often lower than 20% according to an uncertainty analysis. Figure 4 shows typical uncertainty at 115 bars of pressure. Uncertainties are not shown in the remaining figures for the sake of readability.

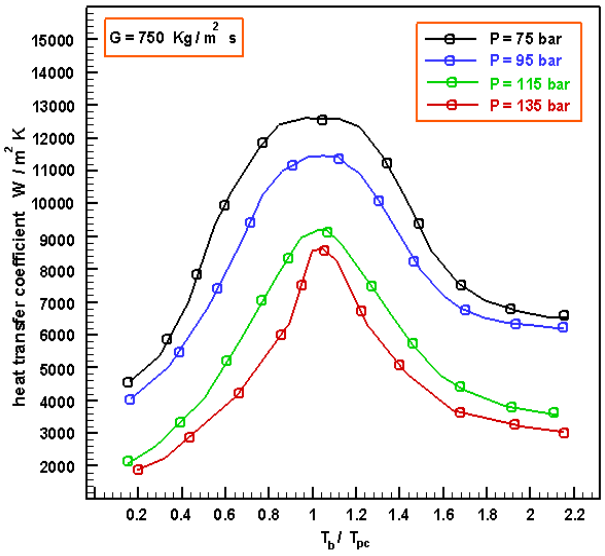

Figure 4 Effect of heat transfer coefficient on pressure as a function of the dimensionless temperature T_b/T_{pc}, Tb is the bulk fluid temperature, upward flow

4.0 RESULTS AND DISCUSSION

By methodically analyzing the impact of the various process variables (pressure, inlet temperature, MF average, and inflow direction) on the HT factor, measurements were made.

4.1 Influence of the Operating Pressure

For working pressures scaling from 75 bars to 135 bars at a specified MF of G = 750 Kg/ m^2 s, for downhill flows, the local HT factor of Carbon dioxide is shown in Figures 4 and 5. Upward inflows exhibit similar phenomena, which were not indicated here. Two alternative feature temperatures are used to indicate the HT factor: (i) the average mass liquid temperature, which is shown in Tb Figure 5 and is equal to:

$$T_b = \frac{(T_{out}+T_{in})_{CO2}}{2} \quad (9)$$

(ii) the mean wall heat degree (Tw Figure 5) computed from the mean mass water heat degree and the water-side HT factor as:

$$T_{w,int} = \frac{Q^{\rightarrow}}{F\alpha_{water}} + \frac{Q^{\rightarrow} \ln(\frac{d_{ext.}}{d_{in.}})}{2\pi l \beta_x} + T_{b,water} \quad (10)$$

The HT factor in the fluid and gas-like zones is essentially constant for all pressures. In this vein, its quantity was dampened with rising pressures and peaks close to the pseudo-critical temperature. In the fluid-like and gas-like zones, the impact of pressure on the precise temperature, and consequently on the HT factor, is weak. These characteristics are associated to the respective evolutions of precise temperature with temperature and pressure. Close the pseudo-critical temperature, the smaller the precise temperature and, thus, the smaller the HT factor, the higher the pressure. The HT factor values are centered at a value around the pseudo-critical temperature T_{pc} when the mass fluid temperature Tb is utilized. The dispersion of the findings for the other characteristic temperatures investigated suggests that the mass liquid temperature Tb is the best choice for simulating changes in the HT factor.

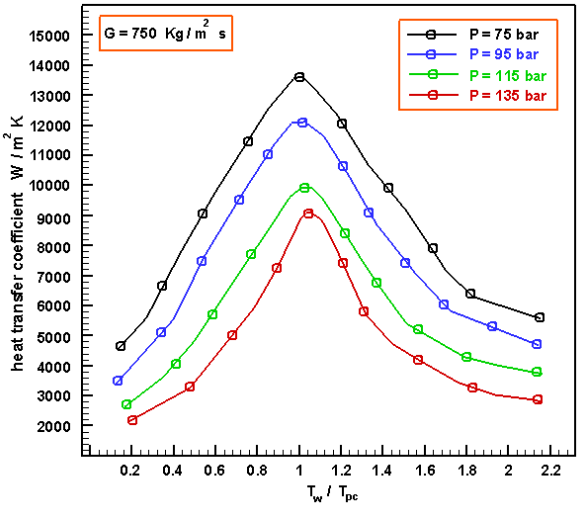

Figure 5 Effect of heat transfer coefficient on pressure as a function of the dimensionless temperature T_w/T_{pc}, T_w, Tw is the wall temperature, upward flow

4.2 Influence of the Mass Flux

Figures 6 and 7 for uphill and downward inflows, respectively, at a working pressure of 100 bars, show how the MF affects the HT factor.

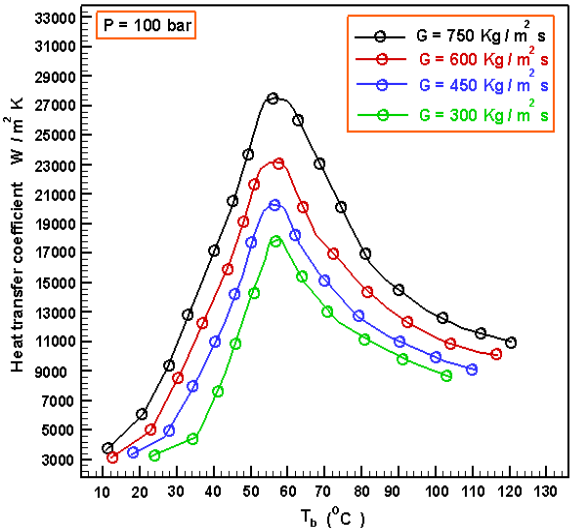

Figure 6 Influence of heat transfer coefficient on mass flux; upward flow

An increment in G leads to an increment in the HT factor of CO_2 for upward inflows, as in the case of a liquid inflow with constant properties, since it enhances turbulent diffusion. According to temperature and MF average, distinct characteristics are seen for downhill inflows. Therefore, the heat transfer coefficient for $T_b \geq T_{pc}$ drops as MF decreases, which is a conventional tendency. When the MF average lowers from 750 Kg/m^2 s to 450 Kg/m^2 s, the HT factor for $T_b \leq T_{pc}$ falls. The MF rate increases in response to subsequent reductions, increasing the HT factor. Such a specific trend, not seen in upward inflows, shows that free convection affects the temperature regime differently.

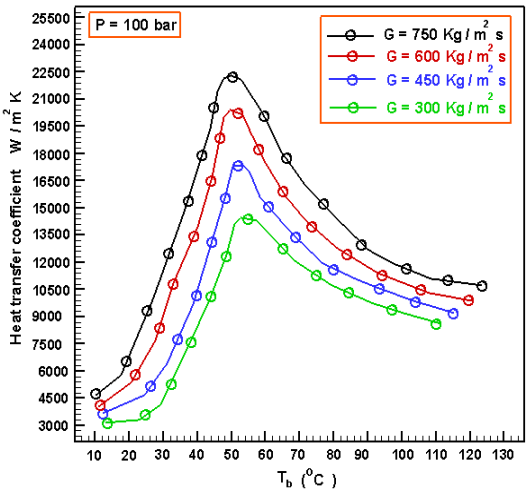

Figure 7 Influence of heat transfer coefficient on mass flux; downward flow

4.3 Influence of Flow Direction/Mixed Convection Effects

Figures 8 and 9 show the general expression of the local HT factor for constant values of MFs of G = 490 kg/m^{2}s and G = 750 kg/m^{2}s, respectively, and for fluctuations in mass liquid heat degree T_b and for various working pressures. For each pressure and MF value, upward and downward inflows were taken into account and contrasted. The HT factor reaches a maximum level in the gas-like zone that is solely dependent on MF velocity. This suggests that the primary method of heat transport is forced convection. Nevertheless, it is impossible to reach a firm conclusion regarding the impact of inflow direction on the HT factor because data for temperatures exceeding 120 oC are not available. For all bulk flows, significant changes in inflow direction are observed in the pseudo-critical zone, which points to a significant role of buoyant forces on heat transfer. The fluid-like zone similarly exhibits comparable behaviors, with the exception of the maximum bulk inflow rate.

The radial density gradient is associated with the start of mixed heat load. According to research on opposing and promoting turbulent composite heat load, respectively, the HT factor is improved in upward inflow and worsened in downward inflow upon composite heat load arises. A mixed heat load variable is used to validate these ideas. The Richardson number, which is given by:

$$\text{Richardson number Ri} = \text{Gr}\, Re^{-2} \qquad (11)$$

Can be used to compare the buoyancy forces with the inertial forces.

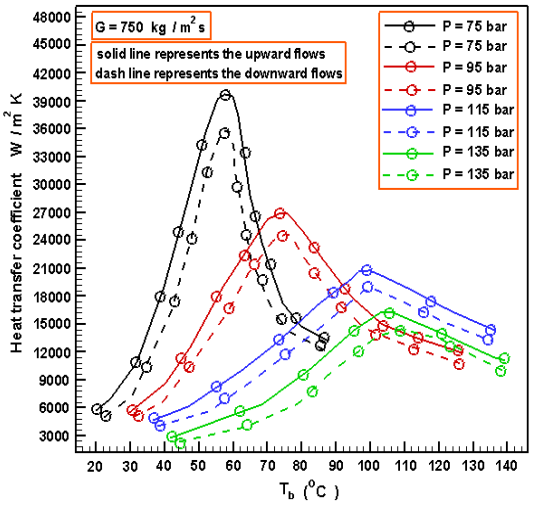

Figure 8 Comparison of heat transfer coefficient for downward and upward flows

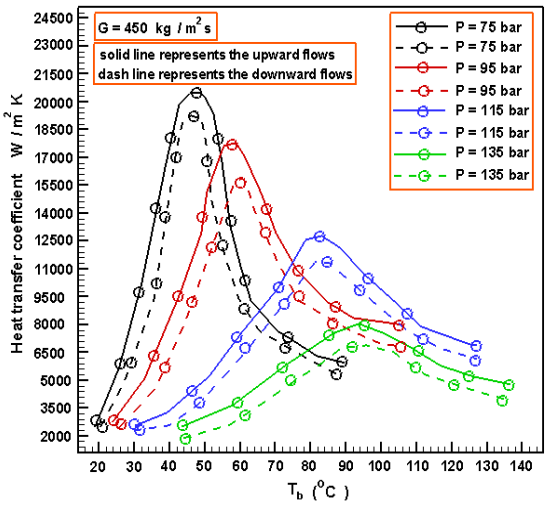

Figure 9 Comparison of heat transfer coefficient for downward and upward flows

To describe the impact of natural heat load on turbulent plumb inflows of heated SC-CO_2, Hall and Jackson [23] created the semi-empirical variable Gr $Gr\, Re^{-2.7}$, whose format is comparable to the Richardson number. Concerning this variable, mixed heat load significantly affects heat transport when:

$$\text{Gr}\, Re^{-2.7} > 10^{-5} \qquad (12)$$

The Reynolds number can be computed utilizing the integral format as follows:

$$Re = [D_h G \times (h_{out} - h_{in})^{-1}] \times \int_{h_{in}}^{h_{out}} \frac{dh}{\mu h} = G \times D_h \times \mu_b^{-1} \quad (13)$$

While Grashof number Gr was computed using the following expression

$$\mathrm{Gr} = \rho_b^2 D^3 g - \rho_{ave} \rho_b D^3 g (\mu_b^2)^{-1} \quad (14)$$

The variation between the mass density and the mean density, which is determined using the estimate suggested by [24], is used in Formula (14 to represent the impact of the radial density gradient, which is the primary factor that ignites buoyant inflows:

$$\rho_{ave} = \frac{\rho_w + \rho_b}{2} \quad if \quad T_w > T_{pc} \quad or \quad T_b < T_{pc}$$

$$\rho_{ave} = \frac{\rho_b T_b - \rho_b T_{pc}}{T_b - T_w} \quad if \quad T_w < T_{pc} < T_b \quad (15)$$

The growth of the mixed heat load factors with the dimensionless heat degree T_b/T^{pc} from high to low MF at various pressures is shown in Figures (10, 11), and (12). In this vein, the limit value of the mixed heat load factors, as defined in [23], is shown as a flat-spotted line shown in Figure 10 for the considerable impact of buoyant forces under heating circumstances. Solely, the data for downward inflows were shown because both upward and downward inflows exhibit identical growth. The inferences made from Figures 8 and 9 were supported. It should be emphasized that for whole taken-in MFs, there is a sizable mixed heat load influence in the pseudo-critical zone. Since buoyant forces merely have a substantial impact on the HT operation for moderate to low MFs in the fluid-like zone, forced heat load predominates for high MFs. Furthermore, whole MFs in the gas-like area was heated primarily by forced heat load. Moreover, the empirical values of the factor in the gas-like zone at G = 300 Kg / m2s are extremely near to the limit value stated by [23], showing that mixed heat load effects were considerable over the all heat degree scale.

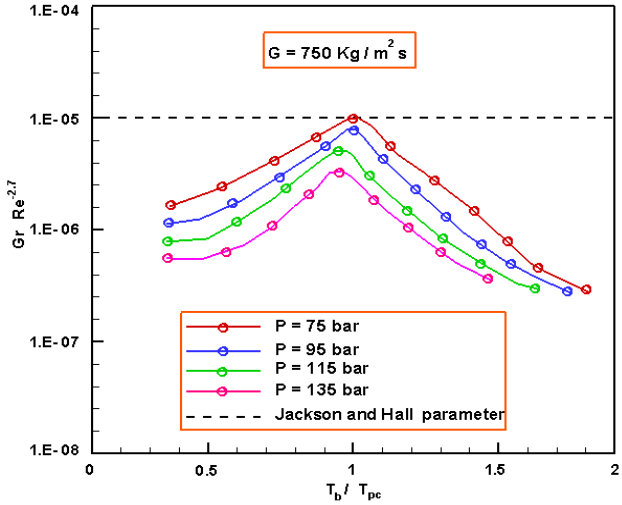

Figure 10 Mixed convection parameter with dimensionless temperature T_b/T_{pc} at G =750 Kg /m²s

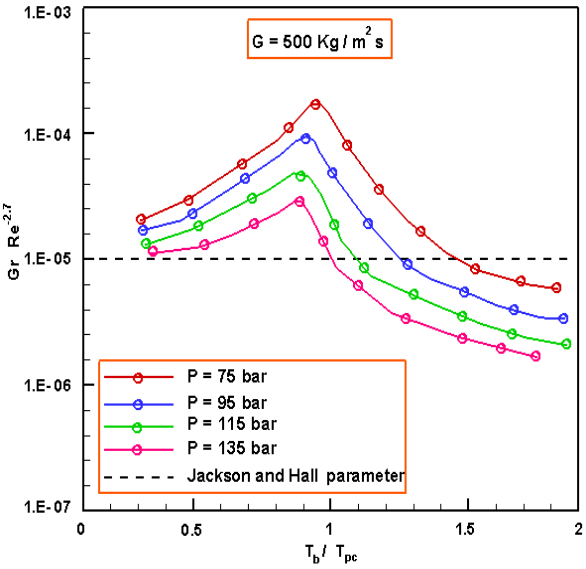

Figure 11 Mixed convection parameter with dimensionless temperature T_b/T_{pc} at G =500 Kg /m²s

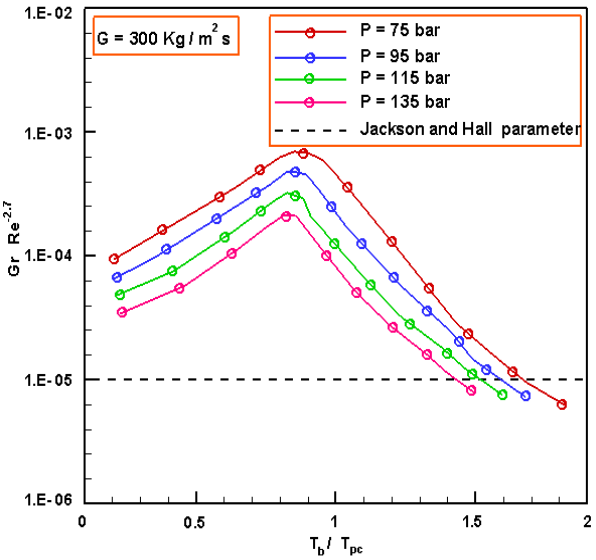

Figure 12 Mixed convection parameter with dimensionless temperature T_b/T_{pc} at G =300 Kg /m²s

Findings were shown in Figure 13 in a dimensionless format that is frequently utilized in research on composite heat load under hot circumstances. Additionally, the empirical Nusselt value is displayed as a function of the previously mentioned composite heat load factor and decreased by a Nusselt value derived from a pure forced heat load relationship. The selected pure forced heat load relationship is the one of Krasnoshchekov revised by [26]:

$$Nu_{\text{forced convection}} = 0.0183 Pr_b^{0.5} Re_b^{0.82} \left(\frac{\rho_b}{\rho_w}\right)^{-0.3} \quad (16)$$

The Prandtl value was computed utilizing the mean typical heat integrated between the mass liquid heat degree and the wall heat point, i.e.:

$$C_{p\,average} = (h_b - h_w) \times (T_b - T_w)^{-1} \quad (17)$$

and

$$\text{Prandtl number}_{\text{average}} = C_{\text{p average}} (h_{\text{out}} - h_{\text{in}})^{-1} \times \int_{h_{\text{in}}}^{h_{\text{out}}} \frac{\mu h}{\omega h}\, dh \quad (18)$$

Upon the Nusselt value being plotted in terms of the variable $\text{Gr} \times \text{Re}^{-2.7}$, single curves for uphill and downward inflows were acheived, respectively. In this context, their shapes resemble those found in composite heat load under heating conditions. Additionally, three distinct thermal regimes may be seen in Figure 13 for instance, forced convection which is the major method of heat transmission at low values of the composite heat load parameter $\text{Gr} \times \text{Re}^{-2.7}$, free heat load has little effect, and the ratio of Nuexp/Nufc is about equal in whole inflow directions. Additionally, this shows good agreement between the empirical results and the forced heat load relationship found in [26]. Thus, as the factor $\text{Gr} \times \text{Re}^{-2.7}$rises, floatation forces become higher and inflow direction variations become apparent. This supports the behaviours that were noticed and depicted in Figures 8 and 9. In this situation, the heat transmission was improved in upward flows (turbulent opposed composite heat load) and worsened in descending inflows (turbulent aiding composite heat load).

Additionally, this can be explained by changes in velocity profiles and the subsequent formation of turbulence as a result of flotation forces. This behaviour is known as "relaminarization" in turbulent composite heat load [27,28]. Moreover, the lowest HT factor quantities, spanning from 2.10^{-5} to 4.10^{-5}, are found for $\text{Gr} \times \text{Re}^{-2.7}$. Maximum values of $\text{Gr}\times\text{Re}^{-2.7}$favour free heat load, and empirical HT agrees well with the practical law established by [25] for SC-CO_2 under heating conditions:

$$\frac{\text{Nu}_b}{\text{Nu}_{FC}} = 15\,(\text{Gr} \times \text{Re}^{-2.7})^{0.4} \quad (19)$$

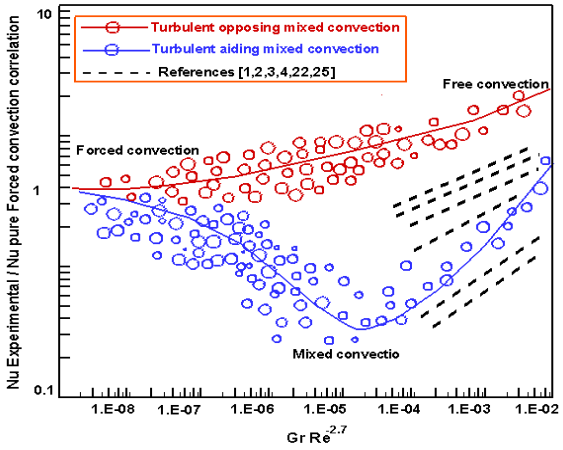

Figure 13 Evolution of mixed convection parameter with Nusselt number to Forced Convection

4.4 Correlations for the Prediction of the Heat Transfer Coefficient

Correlations created for horizontal inflows are the sole fundamental contributions to the estimation of the HT factor of cooled SC-CO_2. In these instances, merely [29] used a relationship that took the Richardson value into account to take into account the impact of composite heat load. Six correlations [1, 2, 3, 4, 22, and 30] , that were generated for SC-CO_2 under cooling conditions were compared to the empirical results.

For a reasonable MF rate of G = 300 kg/m^{2}s, where a considerable impact of floatation force was detected, Figures 14 and 15 compare these predicted methods with our empirical findings. Substantial discrepancies are seen for downhill inflows between the empirical data and the forecasting models, particularly in the fluid-like zone and the pseudo-critical region. Thus, these actions are connected to the growth of composite heat load and, consequently, to the worsening of heat transport brought on by the relaminarization phenomena. A perfect concordance with the relationships created by the above references is seen in the gas-like zone. This demonstrates that inflow direction shouldn't be affected by buoyant forces unless they have a major impact.

The association between the above references Large discrepancies are seen for downhill inflows between the empirical findings and the simulation methods, particularly in the fluid-like zone and the pseudo-critical zone. Thus, these actions are connected to the growth of composite heat load and, accordingly, to the worsening of heat transport brought on by the relaminarization phenomena. A perfect concordance with the relationships created by the above references is seen in the gas-like zone. This demonstrates that inflow direction shouldn't be affected by buoyant forces unless they have a major impact. The association of the above references.

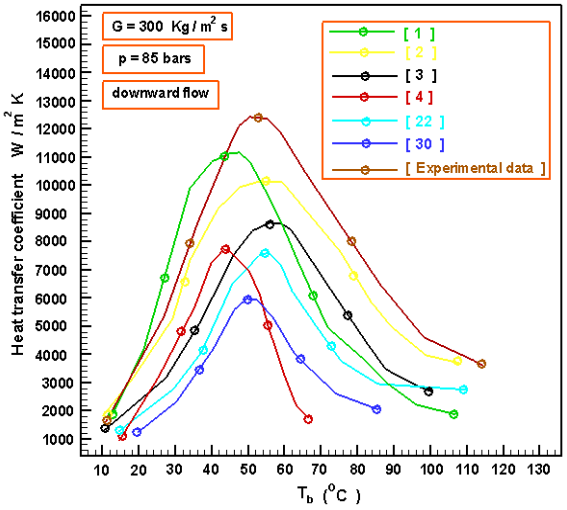

Figure 14 Comparison of measured heat transfer coefficient with various correlations; downward flow

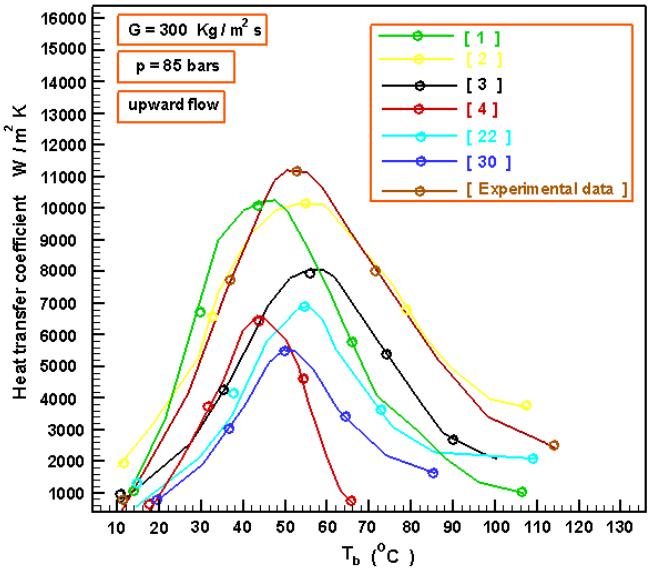

Figure 15 Comparison of measured heat transfer coefficient with various correlations; upward flow

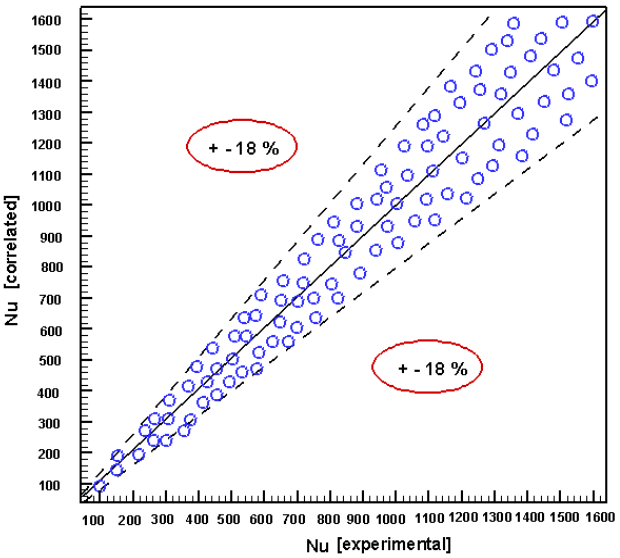

Figure 16 Comparison of the proposed correlation with experimental data , downward flow

The relationships mentioned previously were created for horizontal inflows. The collected information on vertical turbulence assisting and opposing composite heat load under cooling conditions was therefore used to suggest additional relationships. The most acceptable match to our empirical outcomes in turbulent assisted composite heat load, utilizing the [23] variable, results in:

$$\mathrm{Gr}\,Re^{-2.7} < 5.3 \times 10^{-5} \;\; ; \;\; \frac{\mathrm{Nu}_b}{\mathrm{Nu}_{FC}} = 1 - 83 \times (\mathrm{Gr}\,Re^{-2.7})^{0.38} \quad (20)$$

$$\mathrm{Gr}\,Re^{-2.7} > 5.3 \times 10^{-5} \;\; ; \;\; \frac{\mathrm{Nu}_b}{\mathrm{Nu}_{FC}} = 1 - 23 \times (\mathrm{Gr}\,Re^{-2.7})^{0.57} \quad (21)$$

The relationship found in turbulent opposing composite heat load was similar to that found by [28] in SC-CO_2 heating settings. Also, the empirical outcomes were fitted while maintaining the [28] correlation's exponents:

$$\frac{\mathrm{Nu}_b}{\mathrm{Nu}_{FC}} = [1.385 + 5634\,(\mathrm{Gr}\,Re^{-2.7})^{0.74}]^{\frac{1}{5}} \quad (22)$$

Figures 16 and 17 show that the developed relationships are accurate. In opposing composite heat load, where there was high agreement (up to 80% of the 420 valid data points were anticipated within the 13% precision limitations), The precision in assisting composite heat load was roughly 18% owing to the dispersion of empirical outcomes throughout the harmed area. Additionally, information dispersion in turbulent composite heat load that aids in heating was frequently seen in empirical [23,28] and computational [24] research, and it may be due to instability during the relaminarization phenomena.

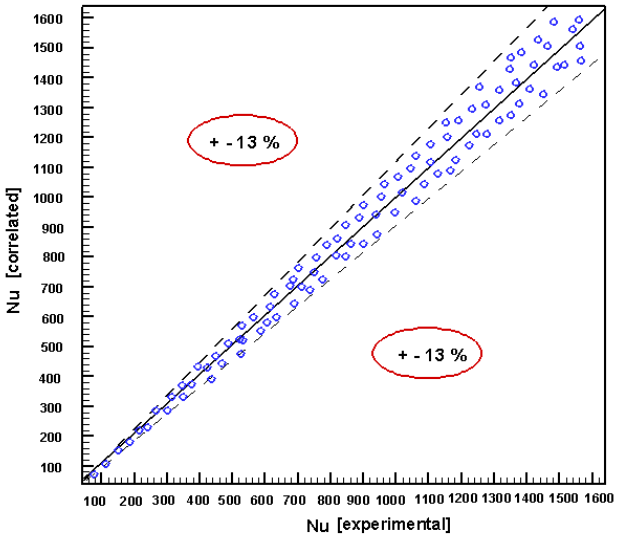

Figure 17 Comparison of the proposed correlation with experimental data , upward flow.

5.0 CONCLUSION

Empirical research was done to examine HT during the cooling of turbulent upward inflows of SC-CO_2. Utilizing particular data reduction techniques, the HT factors were determined, and the impacts of system parameters including pressure, MF, and inflow direction on the HT process were examined. The following summarizes major observations:

Upon the mass temperature reaching near pseudo-critical heat degree Tpc, the HT factor peaks while when the pressure rises, the maximum value falls. In addition, no discernible impact of pressure on the HT factor was seen in the fluid-like or gas-like zones. That is to say, these behaviours are connected to

comparable changes in the specific heat with pressure and temperature.

An increment in MF causes an increment in the HT factor in upward inflows. According to empirical findings, there is an MF velocity threshold below which a reduction increases the HT factor in downhill inflows, in other words, the emergence of composite heat load may explain this.

The impact of inflow direction, and consequently of buoyant forces, can be noticed upon comparing the HT factor for uphill and downhill inflow directly. Such an effect was most noticeable in the fluid-like and pseudo-critical areas. Furthermore, for the lowest values of MF velocity, a potential influence of free heat load could be seen in the gas-like zone.

A similar methodology to that used in the tests under heating situations was used to investigate composite heat load. Utilizing the composite heat load factor and criterion defined by [23], it was specifically determined how the effect of composite heat load might be affected.

Cooling data showed good agreement with empirical findings. Additionally, a visualization of the Nusselt value was made using the dimensionless composite heat load factor. Additionally, both turbulence opposing composite heat load and turbulent assisting composite heat load yielded a single curve. This shows that the thermal behaviour of composite heat load was similar to heating and cooling situations and that the information could be reduced using the selected dimensionless band. Concerning turbulent vertical composite heat load under cooling situations, the current findings fill in the gaps in the previous works.

Finally, for upward and downward inflows, particular relationships were created with the precision of 13% and 18%, correspondingly.

Nomenclature

Cp	Specific heat, J/Kg K
D	Diameter of tube, m
$DQ^{\rightarrow}$	the heat flow rate between cold water and carbon dioxide
s	Length of twisted tape, m
$Q^{\rightarrow}$	flow rate, W
m.	mass flow rate, Kg/s
Nu	Nusselt number
A	area, m^2
T	Temperature , K
G	mass flux, Kg/m^2s
g	gravity of acceleration,m/s^2
Gr	Grashof number
Pr	Prandtl number
Ri	Richardson number
h	specific enthalpy, J /Kg
H	coefficient of heat transfer, W/m^2K

Greek symbol

a	coefficient of heat transfer, W/m^2K
β	conductivity of thermal, $Wm^{-1}K^{-1}$
μ	dynamic viscosity, Pas
ρ	Density, Kg/m^3

Subscript and superscript

CO_2	carbon dioxide
w	water
h	hydraulic
b	bulk
in	inlet
out	outlet
pc	pseudo-critical
ext	external
exp	experimental data
Fc	Force and free convection

References

[1] A.A. Jaddoa , 2021.Convection Heat Transfer Performance For The SCf-CO2 Media In Mini-Tube With Fins Experimentally, *Journal of Engineering Science and Technology*, 16(4), 3407 – 3420.

[2] A.A. Jaddoa,2021. Convection Heat Transfer Analysis with Flow Resistance for Mini-Helically Coiled Tubes at Supercritical Pressures Experimentally, *International Journal of Heat and Technology*, 39(3), 817-824.

[3] A. A. Jaddoa,2022. Experimental investigation of supercritical fluid heat transfer properties in a miniature heat sink, *Journal of Mechanical Engineering*, 19(2), 41-63 .

[4] B. J. Kkihlefa, A.A. Jaddoa, and A. H. Reja,2021. Experimental investigation of heat transfer features for vertical tube using porous media and Carbon dioxide, *Journal of Mechanical Engineering Research and Developments*, 44(5), 188-195.

[5] G. Lorentzen, 1995.The use on natural refrigerants: a complete solution to the CFC/ HCFC predicaments, *Int. J. Refrig.* 18 (3) , 190–197.

[6] Refprop 7.0, NIST Standard Reference Database 23, Version 7.0.

[7] R. Span, W. Wagner,1996.A new equation of state for CO_2 covering the fluid region from the triple-point temperature to 1100 K at pressures up to 800 MPa, *J. Phys. Chem. Ref.* , 25 (6) ,1509–1596.

[8] V. Vesovic, W.A. Wakeham,1990. The transport properties of carbon dioxide, *J. Phys. Chem. Ref.* ,19 (3) , 1509–1596.

[9] M.H. Kim, J. Pettersen, C.W. Bullard,2003. Fundamentals process and system design issues in CO2 vapor compression systems, *Process Energy Combust. Sci*. 30 , 119–174.

[10] Eter, A., Groeneveld, D., Tavoularis, S., 2016. An experimental investigation of supercritical heat transfer in a three-rod bundle equipped with wire-wrap and grid spacers and cooled by carbon dioxide. *Nucl. Eng. Des.* 303, 173–191.

[11] Zahlan, H., Groeneveld, D., Tavoularis, S., 2015. Fluid-to-fluid scaling for convective heat transfer in tubes at supercritical and high subcritical pressures. *Int. J. Heat Mass Transfer* 73, 274–283.

[12] Zahlan, H., Tavoularis, S., Groeneveld, D., 2015a. A look-up table for trans-critical heat transfer in water-cooled tubes. *Nucl. Eng. Des*. 285, 109–125.

[13] Zahlan, H., Groeneveld, D., Tavoularis, S., 2015b. Measurements of convective heat transfer to vertical

upward flows of CO_2 in circular tubes at near-critical and supercritical pressures. *Nucl. Eng. Des*. 289, 92–107.
[14] Ahmad Eter, Dé Groeneveld, Stavros Tavoularis,2017. Convective heat transfer in supercritical flows of CO2 in tubes with and without flow obstacles, *Nuclear Engineering and Design,* 313 ,162–176.
[15] Xiao-jing Zhua , Rui-zeng Zhanga , Xin Dua , XiaoYub , and Qing-gangQiua, 2022. Experimental study on heat transfer deterioration of supercritical CO_2 in a round tube:A boundary assessment, *International Communications in Heat and Mass Transfer,* 134, , 106055.
[16] Lei Wanga, Yu Cheng , Pana Jin Der, Leeb YanWangc , and Ben-Ran Fud Chin Pane,2020. Experimental investigation in the local heat transfer of supercritical carbon dioxide in the uniformly heated horizontal miniature tubes , *International Journal of Heat and Mass Transfer*, 159, 120136.
[17] Peng cheng ,Gu oShou ,chun Liu ,Jianguo Yan Junhui and Wang Qiao ling Zhang,2020. Experimental study on heat transfer of supercritical CO_2 flowing in a mini tube under heating conditions, *International Journal of Heat and Mass Transfer*, 153, 119623
[18] Wenguang Lia, Zhibin Yua, Yi Wang, Yongliang Li, 2022. Heat transfer of supercritical carbon dioxide in a tube-in-tube heat exchanger-a CFD study, *The Journal of Supercritical Fluids*, 181, 105493.
[19] Ruifeng Penga ,Xi anliang Leia , Ziman Guoa Yahu, Wanga Hu , and ixiong Lia XuZ houb,2022. Forced convective heat transfer of supercritical carbon dioxide in mini-channel under low mass fluxes*, International Journal of Heat and Mass Transfer*, 182, 121919.
[20] Chao Lia, Junhon gHaoa ,Xingce Wanga , Zhihua Gea ,and Xiaoze Dua, 2022. Dual-effect evaluation of heat transfer deterioration of supercritical carbon dioxide in variable cross-section horizontal tubes under heating conditions*, International Journal of Heat and Mass Transfer*, 183, Part A, 122103
[21] T.L. Ngo, Y. Kato, K. Nikitin, T. Ishizuka, M. Utamura,2007. Empirical correlations for heat transfer and pressure drop in a new microchannel hot water supplier, in: *Proceedings of the Heat Set conference*, Chambery, 411–420.
[22] A. Bruch , A. Bontemps , S. Colasson,2009. Experimental investigation of heat transfer of supercritical carbon dioxide flowing in a cooled vertical tube, *International Journal of Heat and Mass Transfer*, 52 , 2589–2598.
[23] J.D. Jackson, W.B. Hall, 1979. Influences of buoyancy on heat transfer to fluids in vertical tubes under turbulent conditions, in: S. Kakaç, D.B. Spalding (Eds.), *Turbulent Forced Convection in Cannels and Bundles, Hemisphere, New York,*.
[24] J.H. Bae, J.Y. Yoo,2005. Direct numerical simulation of turbulent supercritical flows with heat transfer, *Phys. fluids* 17 , 1–24.
[25] B.S. Petukhov, L.I. Roizen,1964. Gereralized relationships for heat transfer in a turbulent flow of a gas in tubes of annular section, *High Temp.* 2 , 65–68.
[26] J.D. Jackson, W.B. Hall,1979. Forced convection heat transfer to fluids at supercritical pressures, in: Turbulent Forced Convection in Channels and Bundles, *Hemisphere,* 2, New York, 563–611.
[27] T. Aicher, H. Martin,1997 New correlations for mixed turbulent natural and forced convection heat transfer in vertical tubes, *Int. J. Heat Mass Transfer* 40 (15) , 3617–3626.
[28] J. Fewster,1976. Mixed convection and free convective heat transfer to supercritical pressure fluids flowing in vertical tubes, Ph.D. Thesis, University of Manchester.
[29] S.M. Liao, T.S. Zhao,2002. Measurements of heat transfer coefficients from supercritical carbon dioxide flowing in horizontal mini/micro channels, *J. Heat Transfer* 124 , 413–420.
[30] C.-H. Son, S.-J. Park,2006. An experimental study on heat transfer and pressure drop characteristics of carbon dioxide during gas cooling process in a horizontal tube*, Int. J. Refrig*. 29 (4) ,539–546.

Appendix

The empirical components were equipped with several various sensor recording apparatuses for monitoring heat degree, pressure, inflow velocity, and degree of input temperature, as shown in Table 1 . In line with the experimental procedure, these sensor devices were adopted to lower the uncertainties of estimated different required parameters needs such as heat flow, small channel wall heat degree, mass liquid heat degree, and HT factor at the sensor stage.

Table 1 Experimental structure instrumentation data based on non certainly anticipation

Instrument	Location	Supplier	Model	Serial	Uncertainty	Span
Press. Trans.	Pump Outlet	OMEGA	PX-309-3KGI	071814DO42	±0.25% FS	0 to 3000 PSI
Press. Trans.	Test Section Inlet	OMEGA	MMA2.5K V10 P4COT3A5E	432727	±0.20% FS	0 to 2500 PSI
Thermocouple	Test Section Flux Meter	OMEGA	KMQSS-02U-6	-	±1.1 °C OR ±0.4%	-200 to 1250 °C
Thermocouple	Test Section Inlet/Outlet	OMEGA	TMQSS-062U-6	-	±0.5 °C OR ±0.4%	-250 to 350 °C
Mass Flow Meter	Supercritical Fluid Loop	TRICOR	TCM-0325-FK-SGSS-CADS	1305525	±0.1% Rdng	0 to 325 kg hr-1
Wattage Meter	Test Section Flux Meter	Ohio Semitronics	GW5-103E	16060602	±0.2% Rdng	0 to 100 W